NUMERICAL INTEGRATION OF THE PRIMITIVE EQUATIONS ON THE HEMISPHERE

NORMAN A. PHILLIPS

Massachusetts Institute of Technology, Cambridge, Mass.

[Manuscript received July 6, 1959; revised August 31, 1959]

ABSTRACT

A 48-hr. forecast for the entire Northern Hemisphere of a barotropic hydrostatic atmosphere is made with the "primitive equations." Overlapping Mercator and stereographic grids are used, together with the finite-difference scheme proposed by Eliassen. Initial data corresponded to a Haurwitz-type pattern of wave number 4. The initial wind field was nondivergent and the initial geopotential field satisfied the balance equation. The computations seem to be stable and well behaved, except for two small temporary irregularities. The amplitude of the gravity-inertia waves present in the forecast geopotential field is about 1/30 that of the large-scale field. It can be shown that this is due to the neglect, in the initial data, of the quasi-geostrophically conditioned divergence field. The computational technique itself therefore does not give any unreal prominence to the "meteorological noise." The computational characteristics and stability criterion of the Eliassen finite-difference system are investigated for a linearized version of the equations.

1. INTRODUCTION

The so-called "primitive equations" have not been used much in numerical forecasting because of two main difficulties. First, if the initial wind and pressure fields are not known accurately, artificially large gravity waves will appear in the forecast [3,8]. Secondly, the computational stability criterion for these equations requires a time step of at most 10 minutes compared to the 40- to 60-minute time step allowed in the geostrophic system. The development of larger and faster computing machines is rapidly eliminating the second difficulty. It also seems probable that a gradual improvement of the rawin and radiosonde network, combined with special analyses of the initial data, may go far toward solving the first difficulty. A stable and accurate computation scheme is then all that will be required to take advantage of the more faithful reproduction of atmospheric processes which is possible with the primitive equations. (The geostrophic system not only fails at short wavelengths [2], but also loses its special prognostic value at extremely long wavelengths [1]. In addition, certain important effects such as the horizontal variation of static stability cannot be incorporated into the geostrophic system [10,11].)

There are two aspects to the design of a good computation scheme for the primitive equations: (a) the finite difference equivalents of the partial differential equations themselves, and (b) the formulation of lateral boundary conditions. Eliassen [6] and Platzmann [15] have discussed the former and have arrived at a finite-difference scheme for the primitive equations which is more efficient than the type of finite-differences currently used in geostrophic forecasts. However, boundary conditions for the solution of the primitive equations by finite-differences also require considerable care in their formulation, as has been pointed out, for example, by Smagorinsky [17]. This problem is greatly simplified if the lateral boundary of the forecast region can be placed on the equator, where suitable symmetry assumptions can be imposed on the forecast variables. Although the equator as a boundary is readily fitted into either a spherical coordinate system or into coordinates on a Mercator map, both of these coordinate systems have singularities at the North Pole.

In an attempt to avoid this problem, the writer has suggested the simultaneous use of a Mercator map in low latitudes and a stereographic projection in high latitudes [13]. However, the computational stability of this system is then too complicated a question to be examined by mathematical analysis. A numerical test of the scheme has therefore been made and the results are described in this paper. The equations used were those appropriate to a homogeneous incompressible atmosphere moving hydrostatically. The initial wind and pressure (geopotential) fields were defined mathematically, rather than being obtained from a weather map. The computations are therefore a test only of this method of computation, and do not purport to answer the question of whether adequate initial data can be defined for real forecasts.

2. THE EQUATIONS OF MOTION

The horizontal equations of motion in spherical coordinates, assuming hydrostatic balance and neglecting friction, can be written

$$a\ddot{\lambda}\cos\theta=2a\dot{\theta}(\dot{\lambda}+\Omega)\sin\theta-\frac{1}{a\cos\theta}\frac{\partial\phi}{\partial\lambda}, \tag{1}$$

$$a\ddot{\theta}=-a\dot{\lambda}\cos\theta(\dot{\lambda}+2\Omega)\sin\theta-\frac{1}{a}\frac{\partial\phi}{\partial\theta}. \tag{2}$$

Here λ=longitude, θ=latitude, a=radius of the earth, Ω=angular velocity of the earth, and ϕ=the geopotential of an isobaric surface. The dot ($\dot{}$) is the substantial derivative:

$$(\dot{})=\frac{d}{dt}=\frac{\partial}{\partial t}+\dot{\lambda}\frac{\partial}{\partial\lambda}+\dot{\theta}\frac{\partial}{\partial\theta}+\dot{p}\frac{\partial}{\partial p}. \tag{3}$$

Here p is the pressure, and it is clear that the independent variables which are being used are λ, θ, p, and t. Equations (1) and (2) do not contain the Coriolis term $2\Omega\dot{a}\cos\theta$ or the inertia terms $2\dot{\lambda}\dot{a}\cos\theta$ and $2\dot{a}\dot{\theta}$. They must be neglected for consistency when the hydrostatic approximation is used, since their counterparts in the third equation of motion have also been neglected.

Applying these equations to the motion of an incompressible homogeneous atmosphere with a free surface we find that (1) and (2) carry over as written, if ϕ is set equal to gz, where z is the variable depth of the atmosphere. (3) becomes simpler by the disappearance of the $\partial/\partial p$ operator, since $\dot{\lambda}$ and $\dot{\theta}$ may be taken as independent of the vertical coordinate p. The only other equation needed is the continuity equation, which for this atmosphere can be written

$$\frac{\partial\phi}{\partial t}=-\operatorname{div}(\phi\mathbf{v})=-\frac{\partial(\phi\dot{\lambda})}{\partial\lambda}-\sec\theta\frac{\partial(\phi\dot{\theta}\cos\theta)}{\partial\theta}. \tag{4}$$

(Here g, the acceleration of gravity, has been assumed constant, and variations in a have also been neglected.)

We now define the map coordinates for the Mercator and stereographic projections as follows:

$$\text{Mercator:}\begin{cases}X=a\lambda,\\ Y=-a\ln h,\end{cases} \tag{5}$$

$$\text{Stereographic:}\begin{cases}x=2ah\cos\lambda,\\ y=2ah\sin\lambda,\end{cases} \tag{6}$$

$$h=\cos\theta(1+\sin\theta)^{-1}. \tag{7}$$

Following the procedure outlined in [13], we define

$$\begin{aligned}U&=a\dot{\lambda}\cos\theta=M^{-1}\dot{X},\\ V&=a\dot{\theta}=M^{-1}\dot{Y},\\ M&=\sec\theta,\end{aligned} \tag{8}$$

so that U and V are the horizontal velocity components along the X- and Y-axes of the Mercator projection. M is the scale factor for this projection.

For the stereographic projection we define

$$\begin{aligned}u&=-a\dot{\lambda}\cos\theta\sin\lambda-a\dot{\theta}\cos\lambda=m^{-1}\dot{x},\\ v&=a\dot{\lambda}\cos\theta\cos\lambda-a\dot{\theta}\sin\lambda=m^{-1}\dot{y},\\ m&=2(1+\sin\theta)^{-1},\end{aligned} \tag{9}$$

so that u and v are the horizontal velocity components along the x- and y-axes of the stereographic projection. m is the scale factor for this projection. (U, V) and (u, v) are related by the expressions:

$$\begin{aligned}u&=-U\sin\lambda-V\cos\lambda,\\ v&=U\cos\lambda-V\sin\lambda.\end{aligned} \tag{10}$$

The two horizontal equations of motion and the continuity equation (4) can now be written in the map coordinates:

$$\frac{\partial U}{\partial t}=-M\left[\frac{\partial\phi}{\partial X}+U\frac{\partial U}{\partial X}+V\frac{\partial U}{\partial Y}\right]+V\sin\theta\left[2\Omega+\frac{MU}{a}\right], \tag{11}$$

$$\frac{\partial V}{\partial t}=-M\left[\frac{\partial\phi}{\partial Y}+U\frac{\partial V}{\partial X}+V\frac{\partial V}{\partial Y}\right]-U\sin\theta\left[2\Omega+\frac{MU}{a}\right], \tag{12}$$

$$\frac{\partial\phi}{\partial t}=-M^2\left[\frac{\partial}{\partial X}\left(\frac{U\phi}{M}\right)+\frac{\partial}{\partial Y}\left(\frac{V\phi}{M}\right)\right], \tag{13}$$

$$\frac{\partial u}{\partial t}=-m\left[\frac{\partial\phi}{\partial x}+u\frac{\partial u}{\partial x}+v\frac{\partial u}{\partial y}\right]+v\left[2\Omega\sin\theta-\frac{(xv-yu)}{2a^2}\right], \tag{14}$$

$$\frac{\partial v}{\partial t}=-m\left[\frac{\partial\phi}{\partial y}+u\frac{\partial v}{\partial x}+v\frac{\partial v}{\partial y}\right]-u\left[2\Omega\sin\theta-\frac{(xv-yu)}{2a^2}\right], \tag{15}$$

$$\frac{\partial\phi}{\partial t}=-m^2\left[\frac{\partial}{\partial x}\left(\frac{u\phi}{m}\right)+\frac{\partial}{\partial y}\left(\frac{v\phi}{m}\right)\right]. \tag{16}$$

The Mercator equations (11)–(13) are equivalent to the stereographic equations (14)–(16) and also to the spherical equations (1)–(4).

Equations (11)–(13) have a singularity at the pole where M=sec θ becomes infinite. Equations (14)–(16) have a singularity at the south pole, where $m=2(1+\sin\theta)^{-1}$ becomes infinite. As described in [13], the finite-difference solution of (11)–(16) is to be carried out over one hemisphere by applying (11)–(13) on a Mercator grid in low latitudes and (14)–(16) on a stereographic grid in high latitudes. The Mercator grid should extend from the equator to about 43° latitude, with the stereographic grid being responsible for the area poleward of this latitude (see fig. 1). The singularities are thereby avoided

3. FINITE-DIFFERENCE EQUATIONS

To solve (11)–(16) we use the finite-difference scheme proposed by Eliassen [6] for the primitive equations. To describe this scheme in the present context we must define *four* lattices on the Mercator map and *four* on the stereographic. First we introduce the constant space increment Δ to be used on both maps:

$$\Delta=\frac{2\pi a}{P},\ (P=\text{integer}). \tag{17}$$

The finite difference coordinates will be (p, q) and (i, j):

$$\text{Mercator:}\begin{cases} X=(p-p_0)\Delta,\ p=0,\ 1,\ \ldots,\ P+1, \\ Y=(q-q_0)\Delta,\ q=0,\ 1,\ \ldots,\ Q+1. \end{cases} \tag{18}$$

$$\text{Stereographic:}\begin{cases} x=(i-i_0)\Delta,\ i=0,1,\ \ldots,\ I+1, \\ y=(j-j_0)\Delta,\ j=0,1,\ \ldots,\ I+1. \end{cases}$$

(It will be convenient to take I as an even integer.) The Mercator grid is therefore rectangular $(P+2)\times(Q+2)$ and the stereographic grid is square $(I+2)\times(I+2)$. The numbers (p_0, q_0) and (i_0, j_0) determine the location on the map of the origin of each grid. We define the four Mercator and the four stereographic grids (denoted by A, B, C, and D) by the four sets of values of (p_0, q_0) and (i_0, j_0) shown in table 1. Figure 2 shows the relative orientation on the map of the points on the four grids which have the same subscripts (p, q) or (i, j). From the definition of X in (5) and Δ in (17), it can be seen that the points $p=0$ and $p=1$ on the Mercator grid are identical with the points $p=P$ and $p=P+1$, respectively. These extra points are included in the grids merely for convenience in solving the equations.

The Eliassen computation scheme is obtained by defining the variables (U, V, ϕ) or (u, v, ϕ) on the grids as follows. At time $t=\Delta t, 2\Delta t, 3\Delta t, \ldots, n\Delta t$, U (or u) is represented at the lattice points of grid B; V (or v) is represented at the lattice points of grid C; and ϕ (or ϕ) is represented at the lattice points of grid A. At the intermediate times, $t=1/2\Delta t, 3/2\Delta t, 5/2\Delta t, \ldots, (n+1/2)\Delta t$, U (or u) is represented on grid C, V (or v) on grid B, and ϕ (or ϕ) on grid D. Such an arrangement is much more efficient than when all quantities (e.g. U, V, and ϕ) are defined at *each* point of a single grid at *all* time steps. (Note the discussion of fig. 5 in section 7.) For convenience in notation we will hereafter use a prime superscript (U', V', ϕ', u', v', ϕ') to indicate the quantities defined at the intermediate times $t=1/2\Delta t, \ldots, (n+1/2)\Delta t$. For example, ϕ_{pqn} will indicate $\phi[X=(p-1/2)\Delta, Y=(q-1/2)\Delta, t=n\Delta t]$ (stored on grid A, where $p_0=1/2$ and $q_0=1/2$). ϕ'_{pqn}, however, will indicate $\phi[X=p\Delta, Y=(q-1)\Delta, t=(n+1/2)\Delta t]$ (stored on grid D, where $p_0=0$ and $q_0=1$.)

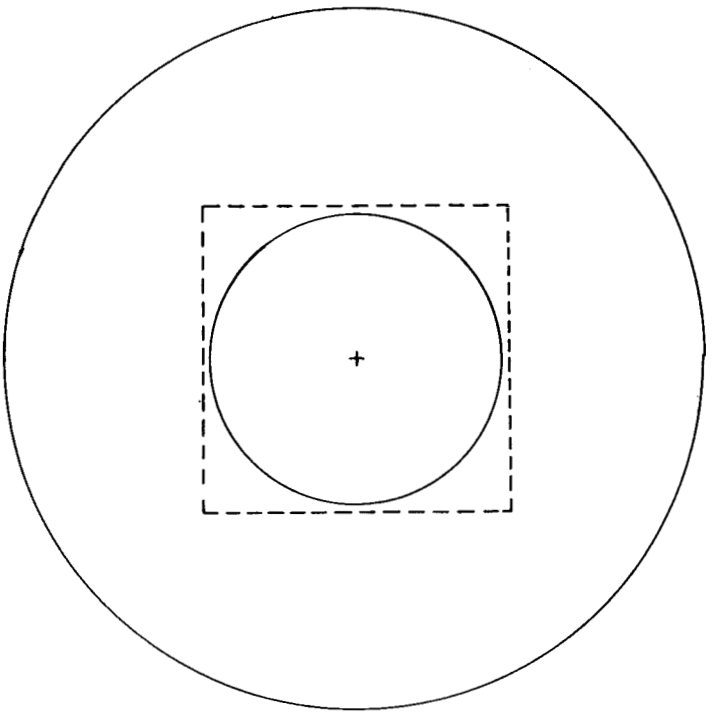

FIGURE 1.—General orientation of Mercator and stereographic grids, shown on a stereographic projection. The stereographic grid covers the square dashed area centered at or near the pole. A Mercator grid covers the area between the equator (outer circle) and the inner circle.

TABLE 1.—*Origin coordinates of the four grids used in the Eliassen finite-difference scheme.*

Grid	p_0	q_0	i_0	j_0
A	1/2	1/2	$I/2+3/4$	$I/2+1/4$
B	1/2	1	$I/2+3/4$	$I/2+3/4$
C	0	1/2	$I/2+1/4$	$I/2+1/4$
D	0	1	$I/2+1/4$	$I/2+3/4$

For convenience in writing the finite-difference equivalents of (11)–(16) we also introduce the notation δ_p and σ_p for the following operators:

$$\delta_p S_{pq}=S_{pq}-S_{p-1\,q},$$

$$\sigma_p S_{pq}=\tfrac{1}{2}(S_{pq}+S_{p-1\,q}).$$

Similar definitions hold for δ_q, σ_q, δ_i, δ_j, σ_i, and σ_j. Finally, to eliminate unnecessary repetition of letter subscripts in the formulae, a quantity such as S_{pq} will be written simply as S_{00}, $S_{p\,q+1}$ as S_{01}, etc.

In the Eliassen scheme, the six equations (11)–(16) applied to the Mercator and stereographic projections, result in 12 finite-difference equations. Quantities appearing on the right side of these equations are understood to have the time subscript n in all cases. The symbol f

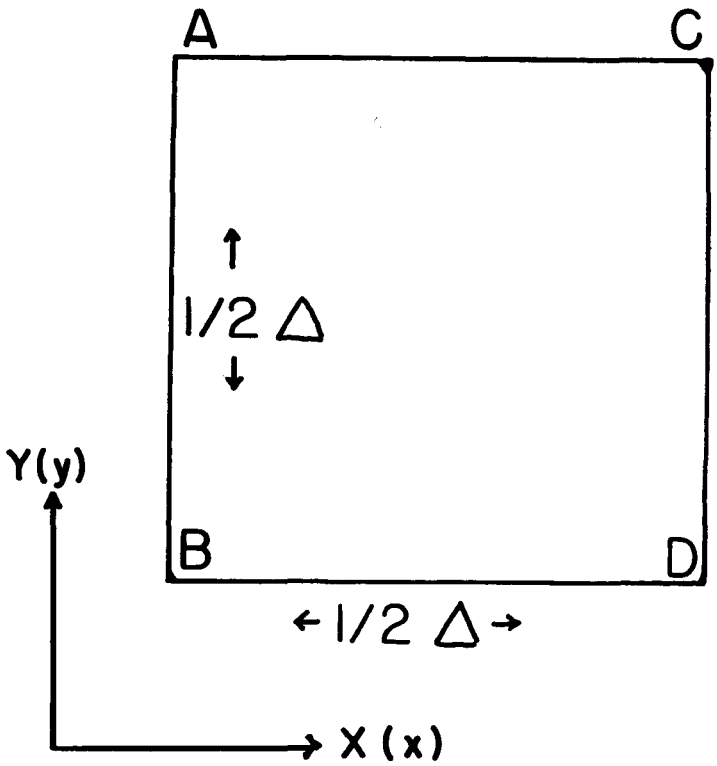

FIGURE 2.—Relative positions on a Mercator (or stereographic) map of the points on the four grids A, B, C, and D which have the same finite-difference coordinates p, q (or i, j).

is used for the Coriolis parameter $2\Omega \sin\theta$. f and the scale factors M and m are identified by additional subscripts A, B, C, or D denoting the grid on which they are located.

$$U'_{00n}-U'_{00\,n-1}=-M_{00C}\left(\frac{\Delta t}{\Delta}\right)\{\delta_p\phi_{10}+\sigma_q[(\sigma_pU_{11})(\delta_pU_{11})]+V_{00}\delta_q\sigma_pU_{11}\}+V_{00}\Delta t f_{00C}\left[1+\left(\frac{M_{00C}}{2\Omega a}\right)\sigma_p\sigma_qU_{11}\right], \quad (19)$$

$$V'_{00n}-V'_{00\,n-1}=-M_{00B}\left(\frac{\Delta t}{\Delta}\right)\{\delta_q\phi_{00}+U_{00}\delta_p\sigma_qV_{00}+\sigma_p[(\sigma_qV_{00})(\delta_qV_{00})]\}-U_{00}\Delta t f_{00B}\left[1+\left(\frac{M_{00B}}{2\Omega a}\right)U_{00}\right], \quad (20)$$

$$\phi'_{00n}-\phi'_{00\,n-1}=-M^2_{00D}\left(\frac{\Delta t}{\Delta}\right)\left\{\delta_p\left[U_{10}\sigma_q\left(\frac{\phi_{10}}{M_{10A}}\right)\right]+\delta_q\left[V_{00}\sigma_p\left(\frac{\phi_{10}}{M_{10A}}\right)\right]\right\}, \quad (21)$$

$$U_{00\,n+1}-U_{00n}=-M_{00B}\left(\frac{\Delta t}{\Delta}\right)\{\delta_p\phi'_{00}+\sigma_q[(\sigma_pU'_{00})(\delta_pU'_{00})]+V'_{00}\delta_q\sigma_pU'_{00}\}+V'_{00}\Delta t f_{00B}\left[1+\left(\frac{M_{00B}}{2\Omega a}\right)\sigma_p\sigma_qU'_{00}\right], \quad (22)$$

$$V_{00\,n+1}-V_{00n}=-M_{00C}\left(\frac{\Delta t}{\Delta}\right)\{\delta_q\phi'_{01}+U'_{00}\delta_p\sigma_qV'_{11}+\sigma_p[(\sigma_qV'_{11})(\delta_qV'_{11})]\}-U'_{00}\Delta t f_{00C}\left[1+\left(\frac{M_{00C}}{2\Omega a}\right)U'_{00}\right], \quad (23)$$

$$\phi_{00\,n+1}-\phi_{00n}=-M^2_{00A}\left(\frac{\Delta t}{\Delta}\right)\left\{\delta_p\left[U'_{00}\sigma_q\left(\frac{\phi'_{01}}{M_{01D}}\right)\right]+\delta_q\left[V'_{01}\sigma_p\left(\frac{\phi'_{01}}{M_{01D}}\right)\right]\right\}, \quad (24)$$

$$u'_{00n}-u'_{00\,n-1}=-m_{00C}\left(\frac{\Delta t}{\Delta}\right)\{\delta_i\phi_{10}+\sigma_j[(\sigma_iu_{11})(\delta_iu_{11})]+v_{00}\delta_j\sigma_iu_{11}\}+v_{00}\Delta t\left\{f_{00C}-\frac{\Delta}{2a^2}[(i-i_0)v_{00}-(j-j_0)\sigma_i\sigma_ju_{11}]\right\}, \quad (25)$$

$$v'_{00n}-v'_{00\,n-1}=-m_{00B}\left(\frac{\Delta t}{\Delta}\right)\{\delta_j\phi_{00}+u_{00}\delta_i\sigma_jv_{00}+\sigma_i[(\sigma_jv_{00})(\delta_jv_{00})]\}-u_{00}\Delta t\left\{f_{00B}-\left(\frac{\Delta}{2a^2}\right)[(i-i_0)\sigma_i\sigma_jv_{00}-(j-j_0)u_{00}]\right\}, \quad (26)$$

$$\phi'_{00n}-\phi'_{00\,n-1}=-m^2_{00D}\left(\frac{\Delta t}{\Delta}\right)\left\{\delta_i\left[u_{10}\sigma_j\left(\frac{\phi_{10}}{m_{10A}}\right)\right]+\delta_j\left[v_{00}\sigma_i\left(\frac{\phi_{10}}{m_{10A}}\right)\right]\right\}, \quad (27)$$

$$u_{00\,n+1}-u_{00n}=-m_{00B}\left(\frac{\Delta t}{\Delta}\right)\{\delta_i\phi'_{00}+\sigma_j[(\sigma_iu'_{00})(\delta_iu'_{00})+v'_{00}\delta_j\sigma_iu'_{00}\}+v'_{00}\Delta t\left\{f_{00B}-\left(\frac{\Delta}{2a^2}\right)[(i-i_0)v'_{00}-(j-j_0)\sigma_i\sigma_ju'_{00}]\right\}, \quad (28)$$

$$v_{00\,n+1}-v_{00n}=-m_{00C}\left(\frac{\Delta t}{\Delta}\right)\{\delta_j\phi'_{01}+u'_{00}\delta_i\sigma_j v'_{11}+\sigma_i[(\sigma_j v'_{11})(\delta_j v'_{11})]\}-u'_{00}\Delta t\left\{f_{00C}-\left(\frac{\Delta}{2a^2}\right)[(i-i_0)\sigma_i\sigma_j v'_{11}-(j-j_0)u'_{00}]\right\}, \quad (29)$$

$$\phi_{00\,n+1}-\phi_{00n}=-m^2_{00A}\left(\frac{\Delta t}{\Delta}\right)\left\{\delta_i\left[u_{00}\sigma_j\left(\frac{\phi'_{01}}{m_{01D}}\right)\right]+\delta_j\left[v'_{01}\sigma_i\left(\frac{\phi'_{01}}{m_{01D}}\right)\right]\right\}. \quad (30)$$

The first six of these refer to the Mercator grid, the second six to the stereographic grid. [The numbers i_0 and j_0 have the value $(I/2+1/4)$ in equations (25) and (29), and the value $(I/2+3/4)$ in equations (26) and (28).]

The order of solving the equations is (19)–(21) and (25)–(27), followed by (22)–(24) and (28)–(30). From the form of the equations it is clear that they can all be solved on the *interior* points of the grids ($p=1, 2, 3, \ldots, P$; $q=1, 2, \ldots, Q$) and ($i=1, 2, 3, \ldots, I$; $j=1, 2, \ldots, I$). A further inspection will show that the left ($i=0$ or $p=0$) and top ($j=I+1$ or $q=Q+1$) boundaries can be computed with equations (21) and (27); the left and bottom ($j=0$ or $q=0$) boundaries can be computed in (19), (23), (25), and (29); the bottom and right ($i=I+1$ or $p=P+1$) boundaries in (24) and (30); and right and top boundaries can be computed in (20), (22), (26), and (28). The remaining boundary values (in general, two adjacent boundaries for each grid of data) must be computed by other means than (19)–(30) in order to regenerate the complete grids of data at each time step. The procedure that was used here is described in the next section.

The system (19)–(30), although written in a form suggestive of uncentered differences, actually uses centered differences. (The truncation error can be expressed as a series in Δ^2 and $(\Delta t)^2$.) A special starting procedure must be used to get the primed variables at time $t=1/2\Delta t$. In the test computation described in this paper, an uncentered step was used to get the initial values of U', V', etc. at $n=0(t=1/2\Delta t)$. U', V', etc. were initially known at $t=0$. Their value at $t=1/2\Delta t(n=0)$ was obtained from (19)–(21) and (25)–(27) by temporarily replacing Δt by $1/2\Delta t$ on the right side of those equations, and the second term on the left side of those equations by $U'(t=0)$, etc.

4. BOUNDARY CONDITIONS

We examine first the equatorial boundary condition, which is used to specify the variables on the bottom row of the Mercator grid ($q=0$). If the motion at one instant $t=t_0$ over the *entire* sphere satisfies the symmetry conditions

$$\begin{aligned}\dot\lambda(\lambda,\theta,t_0)&\equiv\dot\lambda(\lambda,-\theta,t_0),\\ \dot\theta(\lambda,\theta,t_0)&\equiv-\dot\theta(\lambda,-\theta,t_0),\\ \phi(\lambda,\theta,t_0)&\equiv\phi(\lambda,-\theta,t_0),\end{aligned} \quad (31)$$

equations (1)–(4) will preserve this symmetry for all future t. It is clear that under these conditions computations need be made over only one hemisphere, and the appropriate boundary conditions at the equator may be inferred directly from (31). For the Mercator variables U, V, and ϕ, equation (31) may then be written

$$\begin{aligned}U(X,Y,t)&\equiv U(X,-Y,t),\\ V(X,Y,t)&\equiv-V(X,-Y,t),\\ \phi(X,Y,t)&\equiv\phi(X,-Y,t).\end{aligned} \quad (32)$$

As applied to the six Mercator grids of data, we find that this implies

$$\begin{aligned}U'_{p0}&\equiv U'_{p1}\ (q_0=1/2)\\ V'_{p0}&\equiv-V'_{p2}\ (q_0=1)\\ \phi'_{p0}&\equiv\phi'_{p2}\ (q_0=1)\\ U_{p0}&\equiv U_{p2}\ (q_0=1)\\ V_{p0}&\equiv-V_{p1}\ (q_0=1/2)\\ \phi_{p0}&\equiv\phi_{p1}\ (q_0=1/2)\end{aligned} \quad (33)$$

(It can be shown from equations (20) that V'_{p1} will always be zero.)

The left and right boundaries of the Mercator grid are easily handled by applying the cyclic boundary condition that the point ($p=0$, $q=q$) is identical to the point ($p=P$, $q=q$) and the point ($p=P+1$, $q=q$) is identical with the point ($p=1$, $q=q$).

On the top boundary ($q=Q+1$) of the Mercator grids, V', ϕ', and U can be forecast by (20), (21), and (22). The variables U', V, and ϕ at $q=Q+1$ cannot be forecast by (19), (23), and (24), however. (Note that these latter quantities are stored on grids A and C, which have the smaller value of q_0 in table 1, and therefore the most northerly position of the four Mercator grids, as shown by fig. 2.) In addition, boundary values of the six stereographic variables u', v', ϕ', u, v, and ϕ must be obtained on the boundaries listed in the third column of table 2. (These are the only points on those grids which cannot be forecast from the finite difference equations (25)–(30).) In [13] a method was outlined for obtaining these boundary values by interpolation from the associated grid. For example, a Mercator boundary value of ϕ is interpolated from the corresponding stereographic grid of ϕ values, and vice versa. In the case of the velocity components (U, V) and (u, v) the relations (10) must of course be used to supplement the interpolation process, as indicated in the last column of table 2.

TABLE 2.—*Interpolation of boundary values between the Mercator and stereographic grids*

Variable	Grid	Boundaries needed	Interpolated from grid—
U'	Merc. (C)	$q=Q+1$	Ster: u' (C) and v' (F)
ϕ	Merc. (A)	$q=Q+1$	Ster: ϕ (A)
V	Merc. (C)	$q=Q+1$	Ster: u (B) and v (C)
u'	Ster. (C)	$i=I+1$ and $j=I+1$	Merc: U' (C) and V' (B)
v'	Ster. (B)	$i=0$ and $j=0$	Merc: U' (C) and V' (B)
ϕ'	Ster. (D)	$i=I+1$ and $j=0$	Merc: ϕ' (D)
u	Ster. (B)	$i=0$ and $j=0$	Merc: U (B) and V (C)
v	Ster. (C)	$i=I+1$ and $j=I+1$	Merc: U (B) and V (C)
ϕ	Ster. (A)	$i=0$ and $j=I+1$	Merc: ϕ (A)

In order to perform the boundary interpolations in a "neat" manner it is necessary that the individual Mercator and stereographic grids overlap one another to a certain extent. To make this statement more precise, let us define the *sub-boundary* points of a grid as those points located next to a boundary (i.e. where $q=Q$ on the Mercator grids or the points with $i=1$ or I, $j=1$ or I on the stereographic grids). We require that the points $q=Q+1$ on Mercator grids A and C (for which $Y=(Q+1/2)\Delta$) lie *north* of the most northerly sub-boundary point of the stereographic grids. This latter point is located at a distance $r=\sqrt{x^2+y^2}=(\Delta/4)[(2I-3)^2+1]^{1/2}$ from the pole on the stereographic projection. The boundary values of U', ϕ, and V required in table 2 can then be obtained by interpolation on the stereographic grids without reference to the boundary values on those grids. Referring to (5), (6), and (7) we find that Y and r are related by the equation $\exp(-Y/a)=r/2a$. We must therefore have

$$\exp[-(2Q+1)\pi/P]<(\pi/4P)[(2I-3)^2+1]^{1/2}. \quad (34)$$

Another constraint which should be satisfied is that the northernmost boundary point on a stereographic grid (at $r=(\Delta/4)[(2I+1)^2+1]^{1/2}$) be located *south* of the southernmost sub-boundary point on the Mercator grids (located at $q=Q$ on grids B and D, with $Y=(Q-1)\Delta$). The boundary values of u', v', ϕ', u, v, and ϕ required in table 2 on stereographic boundaries can then be obtained by interpolation on the Mercator grids without reference to any Mercator boundary points. This leads to a second inequality:

$$\exp[-(2Q-2)\pi/P]<(\pi/4P)[(2I+1)^2+1]^{1/2}. \quad (35)$$

If Q and I are not large enough to satisfy both (34) and (35), the interpolation process becomes more complicated and will undoubtedly lead to mathematical instabilities.

The values of P, Q, and I used in this test computation were

$$P=80,\ Q=12,\ I=22.$$

This gives a grid increment $\Delta=2\pi a/P$ of 500.4 km. The corresponding distances on the earth varied from 500.4 km. at the pole ($m=1$) and equator ($M=1$) to a minimum of about 350 km. ($m\sim M\sim 1.4$) in middle latitudes. It should be pointed out that horizontal space differences in the system (19)—(30) are taken over the distance Δ, rather than 2Δ as is customary at present in numerical weather prediction.

It might be thought that *all* boundary values on the stereographic grids, including those which can be forecast by (19)–(24), could be obtained by interpolation. This procedure was in fact tried in a preliminary computation. (It is logically easier from the point of view of the machine program to interpolate all four boundaries on the stereographic grids than it is to do only those listed in table 2.) However, the results of this preliminary computation were quite unsatisfactory compared to the results described in this paper. When interpolation was done on all boundaries, the flow patterns tended to move at different speeds on the two grids, and discontinuities developed near the grid boundaries.

The details of the interpolation process were as described in [13]. Computation of one interpolated boundary value took less machine time than did a computation of one of the equations (19)–(30) at one pont. Thus, only about 5 percent of the total computation time was spent on the boundary computations.

5. INITIAL DATA

The initial velocity and geopotential fields for this test computation were defined by a flow pattern of the type treated by Haurwitz [7]. The initial velocity field $\mathbf{v}$ was non-divergent, and given by the stream function ψ:

$$\psi=-a^2\omega\sin\theta+a^2K\cos^R\theta\sin\theta\cos R\lambda. \quad (36)$$

ω, K, R, and a (radius of the earth) are constants. As shown by Haurwitz, a flow pattern like this will, in a *non-divergent* barotropic atmosphere, move from west to east without change of shape with the angular velocity ν:

$$\nu=\frac{R(3+R)\omega-2\Omega}{(1+R)(2+R)}. \quad (37)$$

The equations used in the computations, however, are not those for a non-divergent atmosphere, but for one with a free surface. (37) will therefore only be satisfied approximately. The presence of divergence in the barotropic atmosphere, will, as is well known, slow up the rate of progression of the flow pattern, especially for small values of the wave number R [16].

In the non-divergent barotropic atmosphere treated by Haurwitz, the pressure field (p/ρ) associated with the initial flow pattern (36) can be readily determined by integration of the equations of motion (1)–(2), using the

angular phase velocity ν to evaluate $\partial\psi/\partial t$. We replace p/ρ by ϕ. The distribution of ϕ obtained in this way is given in the following formulae:

$$\phi=\phi_0+a^2A(\theta)+a^2B(\theta)\cos R\lambda+a^2C(\theta)\cos 2R\lambda, \quad (38)$$

$$A(\theta)=\tfrac{1}{2}\omega(2\Omega+\omega)c^2+\tfrac{1}{4}K^2c^{2R}[(R+1)c^2 +(2R^2-R-2)-2R^2c^{-2}],$$

$$B(\theta)=\frac{2(\Omega+\omega)K}{(R+1)(R+2)}c^R[(R^2+2R+2)-(R+1)^2c^2],$$

$$C(\theta)=\tfrac{1}{4}K^2c^{2R}[(R+1)c^2-(R+2)],$$

$$c=\cos\theta.$$

Both (36) and (38) satisfy the symmetry conditions (31). ϕ_0 in (38) is an arbitrary constant which will determine the average height of the free surface in the atmospheric model being used here. This in turn will determine the speed of propagation of gravity-inertia waves and also the order of magnitude of the divergence in the model (div $\mathbf{v}=-\phi^{-1}d\phi/dt$).

The initial distribution of ψ and ϕ used for the computations was that given by (36) and (38), with the following values for the constants:

$$\omega=K=7.848\times10^{-6}\text{ sec.}^{-1}\ (\sim0.1\Omega),$$

$$R=4$$

$$\phi_0=9.8\ (8\times10^3)\text{ m.}^2\text{ sec.}^{-2}.$$

These values for ω and K give rise to large velocities, the maximum values of $a\dot{\lambda}\cos\theta$ $(=-a^{-1}\partial\psi/\partial\theta)$ and $a\dot{\theta}[=(a\cos\theta)^{-1}\partial\psi/\partial\lambda]$ being about 99 and 65 m. sec.$^{-1}$. Figure 3 shows the distribution of the initial height of the free surface $z=\phi/g$. The total variation of 3.5 km. in z is several times as large as the typical variation in the height of the 500-mb. surface in winter.

It is clear from the way in which this initial ϕ-field was determined, that ψ and ϕ together satisfy the so-called "balance equation" [3]:

$$\nabla\cdot F\nabla\psi+\nabla\cdot\mathbf{A}=\nabla^2\phi,$$

where

$$F=\sin\theta\left(2\Omega-\frac{1}{a^2\cos\theta}\frac{\partial\psi}{\partial\theta}\right),$$

$$A_\lambda=a^{-3}\sec\theta J\left(\frac{\psi,\partial\psi/\partial\theta}{\lambda,\theta}\right)=-\mathbf{v}\cdot\nabla(a\dot{\lambda}\cos\theta), \quad (39)$$

$$A_\theta=-a^{-3}\sec\theta J\left(\frac{\psi,\sec\theta\partial\psi/\partial\lambda}{\lambda,\theta}\right)=-\mathbf{v}\cdot\nabla(a\dot{\theta}).$$

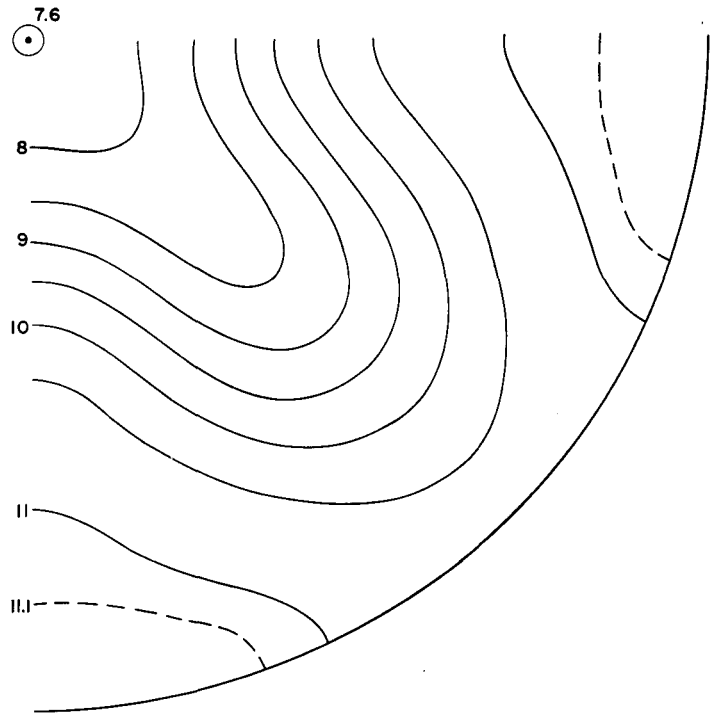

FIGURE 3.—Initial distribution of the height of the free surface, shown on a stereographic projection. Only one octant is shown, the pattern repeating in the other three octants of the hemisphere. The outer circle is the equator. Isolines are labeled in km.

(∇ is the horizontal gradient operator on the sphere.) The advantage of using ϕ- and ψ-fields which satisfy (39) is that $\partial(\text{div }\mathbf{v})/\partial t$ is initially zero. According to Charney [3], this will result in much smaller amplitudes of the gravity-inertia waves than would appear if only the geostrophic relation were used to relate the initial ϕ- and $\mathbf{v}$-fields to one another.

It is of some interest to examine the vorticity field corresponding to (36):

$$f+\zeta=2(\omega+\Omega)\sin\theta-(1+R)(2+R)K\cos^R\theta\sin\theta\cos R\lambda \sim f[1.1-1.5\cos^4\theta\cos 4\lambda]. \quad (40)$$

(We have here introduced the value $R=4$ and the approximate values $\omega=K\sim0.1\Omega$). Because of the large value of K there are four regions of negative absolute vorticity in low latitudes. These regions extend poleward to a latitude of about 22° where $\cos^4\theta=(1.1)/(1.5)$. The minimum value of $f+\zeta$ (reached at $\theta\sim7.25°$) is only about -0.09Ω, however.

6. COMPUTATIONAL STABILITY

The computational stability of the finite-difference equations derived in section 3, with the boundary condi-

tions discussed in section 4, is difficult to investigate because the forecast equations are nonlinear with variable coefficients, and the boundary conditions are not simple. Considerable information can be obtained, however, by examining the computational stability of linearized versions of the forecast equations. To further simplify the analysis we make the coefficients constant and consider only solutions which are periodic in x and y, as on an infinite plane.

As an analogue to (11)–(13) or (14)–(16), we then treat the following simple system:

$$\frac{\partial u}{\partial t}=-\frac{\partial \phi}{\partial x}-u_0\frac{\partial u}{\partial x}-v_0\frac{\partial u}{\partial y}+fv \tag{41}$$

$$\frac{\partial v}{\partial t}=-\frac{\partial \phi}{\partial y}-u_0\frac{\partial v}{\partial x}-v_0\frac{\partial v}{\partial y}-fu \tag{42}$$

$$\frac{\partial \phi}{\partial t}=-\Phi\left(\frac{\partial u}{\partial x}+\frac{\partial v}{\partial y}\right)-u_0\frac{\partial \phi}{\partial x}-v_0\frac{\partial \phi}{\partial y}. \tag{43}$$

Here f, u_0, v_0, and Φ are constants, while u, v, and ϕ are perturbation quantities. (43) could also include a term $-(u\partial\Phi/\partial x+v\partial\Phi/\partial y)=-f(uv_0-vu_0)$. It also is omitted for simplicity. For disturbances of the form $\exp i\ (\mu t+ax+by)$, (41)–(43) are satisfied by three solutions for the frequency μ:

$$\begin{aligned}\mu_1&=-(au_0+bv_0),\\ \mu_2&=\mu_1+[f^2+\Phi(a^2+b^2)]^{1/2},\\ \mu_3&=\mu_1-[f^2+\Phi(a^2+b^2)]^{1/2}.\end{aligned} \tag{44}$$

μ_1 corresponds to a geostrophic, non-divergent wave, while μ_2 and μ_3 are gravity-inertia waves.

We now write (41)–(43) in finite-differences, using the same basic scheme that was used to get (19)–(24) and (25)–(30). We introduce solutions of the form $\Psi_{pq}=\exp i\ (\alpha p+\beta q)$, where $\alpha=a\Delta,\beta=b\Delta$, and p and q are the finite-difference space coordinates. For convenience in the analysis we introduce the following new quantities:

$$\begin{aligned}u_{pqn}&=U_n\sqrt{\Phi}\,\Psi_{pq},\\ v_{pqn}&=V_n\sqrt{\Phi}\,\Psi_{pq}e^{1/2i(\alpha+\beta)},\\ \phi_{pqn}&=H_n\Phi\,\Psi_{pq}e^{1/2i\beta},\\ u'_{pqn}&=U'_n\sqrt{\Phi}\,\Psi_{pq}e^{1/2i(\alpha+\beta)},\\ v'_{pqn}&=V'_n\sqrt{\Phi}\,\Psi_{pq},\\ \phi'_{pqn}&=H'_n\Phi\,\Psi_{pq}e^{1/2i\alpha},\\ W&=\frac{\Delta t}{\Delta}\left(u_0\sin\frac{\alpha}{2}\cos\frac{\beta}{2}+v_0\cos\frac{\alpha}{2}\sin\frac{\beta}{2}\right),\\ F&=\tfrac{1}{2}f\Delta t,\\ M&=\left(\frac{\Delta t}{\Delta}\right)\sqrt{\Phi}\sin\frac{\alpha}{2},\\ N&=\left(\frac{\Delta t}{\Delta}\right)\sqrt{\Phi}\sin\frac{\beta}{2}.\end{aligned} \tag{45}$$

U_n, V_n, . . ., H'_n are now the non-dimensional amplitudes of the perturbations and are functions of time $(n\Delta t)$. We also define the following matrices:

$$Z_n=\begin{pmatrix}U_n\\ V_n\\ H_n\end{pmatrix},\ Z'_n=\begin{pmatrix}U'_n\\ V'_n\\ H'_n\end{pmatrix},$$

$$G=-2i\begin{pmatrix}W & iF & M\\ -iF & W & N\\ M & N & W\end{pmatrix}. \tag{46}$$

The Eliassen-grid finite-difference equivalents of (41)–(42) can then be written (after some algebra) in the following compact form:

$$\begin{aligned}Z'_n&=Z'_{n-1}+GZ_n,\\ Z_n&=Z_{n-1}+GZ'_{n-1}.\end{aligned} \tag{47}$$

An equation for Z (or Z') alone is easily obtained from these:

$$Z_{n+1}-2LZ_n+Z_{n-1}=0. \tag{48}$$

Here L is the matrix $I+\frac{1}{2}G^2$, where I is the unit matrix. L is Hermitian (l_{ij} is the complex conjugate of l_{ji}) and therefore has three real eigenvalues λ_j and three orthogonal eigenvectors ϵ_j. Further calculation shows that the λ's are equal to $\cos\xi$, where ξ can assume any one of the three values

$$\begin{aligned}\sin(\tfrac{1}{2}\xi_1)&=W,\\ \sin(\tfrac{1}{2}\xi_2)&=W-[F^2+M^2+N^2]^{1/2},\\ \sin(\tfrac{1}{2}\xi_3)&=W+[F^2+M^2+N^2]^{1/2}.\end{aligned} \tag{49}$$

Expanding Z_n now as a series in the orthogonal eigenvectors ϵ_j,

$$Z_n=\sum_{j=1}^{3}\delta_{jn}\epsilon_j,$$

we find that (48) leads to the following scalar equations for the δ_j:

$$\delta_{j\ n+1}-(2\ \cos\ \xi_j)\delta_{jn}+\delta_{j\ n-1}=0,\ \mathrm{j}=1,2,3. \tag{50}$$

The solutions for δ_{jn} are therefore

$$\delta_{jn}=\exp\ \pm(i\ n\xi_j), \tag{51}$$

where the three values of ξ_j are still given by (49). Computational stability is achieved by demanding that all ξ_j be real. Referring to (49) we see that this requires the following inequality to be satisfied:

$$|W\pm\sqrt{F^2+M^2+N^2}|<1. \tag{52}$$

It should be noted that a weakening of this to permit the equality will allow $\cos\ \theta=-1$, whereupon (50) will contain an unstable solution of the form $\delta_n=n(-1)^n$.

Introducing the definitions of W, F, M, and N from (45), and taking the worst possible orientation for u_0 and v_0, the simplified computational stability criterion for this Eliassen grid system can finally be written:

$$\left(\frac{\Delta t}{\Delta}\right)\left[|\mathbf{v}_0|+\sqrt{\left(\frac{f\Delta}{2}\right)^2+\Phi}\right]<1. \tag{53}$$

In this formula Δt and Δ are the time and space increments over which the partial derivatives with respect to t and x (or y) are expressed as finite differences. $|\mathbf{v}_0|$ is equal to $\sqrt{u_0^2+v_0^2}$. As is clear from the preceding analysis, the satisfaction of (53) will not necessarily insure the stability of a computation where the lateral boundary conditions are more complicated than the simple ones implied by (45). In such cases (53) is best thought of as a necessary, but not sufficient, condition for stability.

Criterion (53) allows a maximum time step of $\Delta t=$ 12.5 min. to be used in forecasting the flow pattern described in section 5. The test computations were made with a time step of (1/7) hr.$\sim$8.5 min. It took approximately 30 sec. on an IBM 704 to compute one time step; that is, to solve the 12 equations (19)–(30) at all points concerned, and to do the necessary boundary computations listed in table 2. A 24-hr. forecast therefore required about 84 minutes of computer time. (Checking of the results is not included in this figure.) Any further increase in computer speeds, say by a factor of 10, will certainly make it possible to use the primitive equations over an entire hemisphere for even a multi-level baroclinic atmosphere.

It is clear from (51) and (49) that the linearized finite-difference system (47) possesses *six* frequencies. The continuous system (41)–(43), on the other hand, possesses only the *three* frequencies given in (44). It can be shown that three of the six frequencies in the finite-difference system are similar in form to the three continuous frequencies in (44), and that the remaining three finite-difference frequencies differ only by a reversal in the sign of the advection term W. These extra solutions are very similar to the "computational wave" which is present in the conventional way of solving the geostrophic vorticity equation [14].

7. RESULTS OF THE TEST COMPUTATION

A 48-hr. forecast was made from the initial wind and pressure fields given by (36) and (38). Since this forecast cannot be compared with either a real atmospheric flow pattern or a mathematically known solution, the results will be examined only from the following viewpoints:

a. Smoothness of the fields in space. In particular, the agreement between the stereographic and Mercator representations in the areas of overlap (see fig. 1).

b. Smoothness of the fields in time—the question of "meteorological noise."

Figure 4 shows the forecast field of $z=\phi/g$ at 48 hours, in the area covered by the stereographic A grid. The waves have moved about 18° to the east in approximate agreement with (37). Of special interest is the agreement between the stereographic isolines and the Mercator isolines (heavy dashed lines) in the area of overlap of the two grids. In general, the two sets of lines are both smooth. They agree with one another extremely well except for one area near the upper right corner and another smaller area near the lower left corner. The maximum value of the difference between the two grids of z-values in these areas is about 90 meters—about 1/20 of the maximum difference in z between a trough and ridge at the same latitude. The field of z on that portion of the Mercator grid not shown in figure 4 was very smooth, even in the low latitude regions where $f+\zeta$ was negative.

A severe test of the smoothness of the forecast z-field is shown in part A of figure 5. Here the quantity $-4z_{ij}+z_{i+1\ j}+z_{i\ j+1}+z_{i-1\ j}+z_{i\ j-1}$ at $t=$ 36 hr. is plotted for an area centered near the North Pole. (Only the stereographic grid covers this region.) There is some tendency for a "checkerboard" pattern to appear, but it is not very pronounced.

Smagorinsky [17] and Hinkelmann [9] have made experimental forecasts with the primitive equations which were not based on the Eliassen type of finite-difference grid. In their scheme, only one grid is used (instead of the four grids described in section 3), and the geopotential and both velocity components are stored at all points of this single grid at all time steps. Time and space derivatives are expressed as centered finite differences over the intervals $2\ \Delta\ t$ and $2\ \Delta$, much as is done in the usual

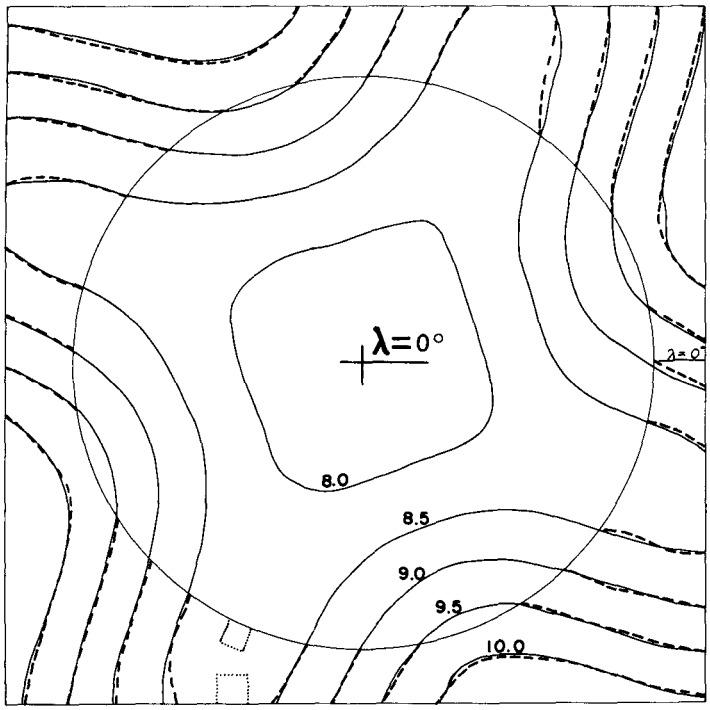

FIGURE 4.—The forecast field of z at 48 hours, drawn on a stereographic map, showing only the area covered by the stereographic grid A. Isolines are drawn at intervals of 500 m. Thin continuous isolines are drawn from the stereographic grid-point values (grid A). Heavy dashed isolines are drawn from the Mercator grid-point values (grid A). The Mercator grid A extended only in to the circle. The small dotted areas show the spacing of the lattice points on the Mercator and stereographic grids.

4	14	6	12	5	-1	12	2	22	-4	22	-4	19	2
5	0	11	5	5	15	10	19	-7	25	-14	22	-7	22
4	2	8	2	21	-4	10	-4	22	-4	27	-4	25	-4
6	17	0	11	1	17	-3	22	-14	27	-20	27	-14	22
5	1	14	3	13	10	13	-4	25	-4	27	-4	22	-4
5	9	5	10	8	4	7	22	-7	22	-14	25	-7	19
6	3	11	8	6	6	8	2	19	-4	22	-4	22	2
			A							B			

FIGURE 5.—Grid point values of the quantity $(-4z_{ij}+z_{i+1\ j}+z_{i-1\ j}+z_{i\ j+1}+z_{i\ j-1})$ at 36 hours for an area centered near the pole; (A) from the forecast made with the Eliassen grid system, (B) from a special forecast made with the finite-difference system used by Smagorinsky and Hinkelmann. Units are in tens of meters.

way of making numerical weather predictions with the geostrophic model [4]. In order to compare this method with the Eliassen method of solving the primitive equations, a special 36-hr. forecast was made with the appropriate difference equations from the same initial flow pattern. Figure 5 B shows the resulting field of $-4z_{ij}+z_{i+1\ j}+z_{i\ j+1}+z_{i-1\ j}+z_{i\ j-1}$ at 36 hr. from this special forecast. The *average* value of the plotted numbers is almost the same, 7.1 in figure 5A and 8.2 in figure 5B, but the range in the plotted values is 25 in figure 5A and 47 in figure 5B. The tendency to a checkerboard pattern is very marked in figure 5B. It is clear then that forecasts made this way will be much more irregular than those obtained with the Eliassen grid system.

The main purpose of the computation described in this paper was to test the computational stability of the overlapping stereographic-Mercator grids, since this feature of the computation was not amenable to the type of computational stability analysis carried out in section 6. Although the results shown in figure 4 certainly indicate that the scheme is at least reasonably stable, two small temporary "wiggles" did appear during the course of the forecast. They did not appear until after 24 hours, and as shown by figure 4, had practically disappeared again by 48 hours. They appeared only near the top boundary of the Mercator grid, the stereographic grid point values being quite smooth at all times. Figure 6 shows the detailed structure at 36 hours of the wiggle located near $\lambda=56°$. The other irregularity was very similar and located exactly on the other side of the hemisphere, in the same part of the wave-like flow pattern.

Both of the irregularities seemed to be quasi-geostrophic in character, with the U and V components following the geopotential field shown in figure 6. The writer has not been able to isolate the cause of these two "errors," which, although small, disfigure what otherwise seens to be an excellent computation. Since they appear only on the Mercator grids, and in only two of the four waves, it is safe to conclude that they do not represent anything real, but represent rather some peculiar type of truncation error. In this connection it may be important to recall from section 6 that the Eliassen grid system does contain three false computational frequencies in addition to the three physical frequencies. Experience with the geostrophic vorticity equation has shown that such false frequencies frequently become important near boundaries.

In order to give an idea of the amount of "meteorological noise" present in the computations, a record of the height z at 2-hour intervals is shown in figure 7 for 3 selected points. (Unfortunately, a record of the forecast fields was printed out only every 2 hours=14 time steps.) Point I is located near the equator in one of the regions of negative $f+\zeta$. Point II is located initially in the trough at 46° N. near the top of the Mercator grid. (It is one of the points in figure 6, where it is marked II.) Point III

is located 175 km. from the North Pole. All three points have been purposely chosen in regions of small net changes in z (except for the last half of curve II), so that any small short-period oscillations will stand out clearly. Such oscillations are indeed present and evidently have an amplitude corresponding to a height change of ± 50 meters. For comparison, the maximum net 48-hr. change in z at any point was equal to ± 1450 meters—a value 29 times as large as the amplitude of the meteorological noise. Height tendencies measured over intervals of less than about 4 hours would therefore represent primarily "noise," and not the slower quasi-geostrophic changes.

This result—the presence of a small but noticeable inertia-gravity oscillation—is at first sight contrary to the results obtained from "balanced" initial data by Charney in [3]. In Charney's test computation with the primitive equations, no meteorological noise appeared at all when the initial wind and pressure fields satisfied the balance equation (39). The explanation for this difference is that Charney's initial flow pattern was a stationary wave, while the flow pattern used here is not stationary but moves slowly to the east. In a barotropic atmosphere a quasi-geostrophic wave has, as is well known, a small, but significant divergence field associated with it if the wave is not stationary. This divergence associated with the geostrophic wave disappears only if the wavelength happens to be such that the wave is stationary. Therefore, unless the initial wind field also has this small amount of divergence, the forecast must contain some high-frequency gravity-inertia oscillations ("noise") in addition to the low-frequency geostrophic motions.

From the linearized treatment of the noise problem by Hinkelmann in [8], it is possible to estimate the magnitude of the noise which is introduced by neglecting in the initial data the (small) divergence associated with a moving geostrophic wave. If c_1 and c_2 are the phase velocities of the geostrophic and gravity-inertia waves respectively, the fictitious gravity-inertia wave will have an amplitude in the geopotential ϕ approximately equal to (c_1/c_2) times the amplitude in ϕ of the quasi-geostrophic wave. For the example treated in this paper, (c_1/c_2) is about 1/30, giving good agreement with the numerically computed amplitudes in ϕ of the two types of motion. There can be no doubt then that the numerically computed noise shown in figure 7 is due to the choice of initial data and is not caused by the numerical technique. The importance of including this geostrophically-conditioned divergence in the initial data for the primitive equations has also been demonstrated recently by Hinkelmann [9].

According to the theory of the geostrophic approximation as developed by Monin [12] (contained to some extent also in [5]), the second geostrophic approximation to the true wind is given by $\mathbf{v}_2$, say, where the divergence of $\mathbf{v}_2$ is precisely that divergence which appears (multiplied by f) in the usual geostrophic form of the vorticity equation,

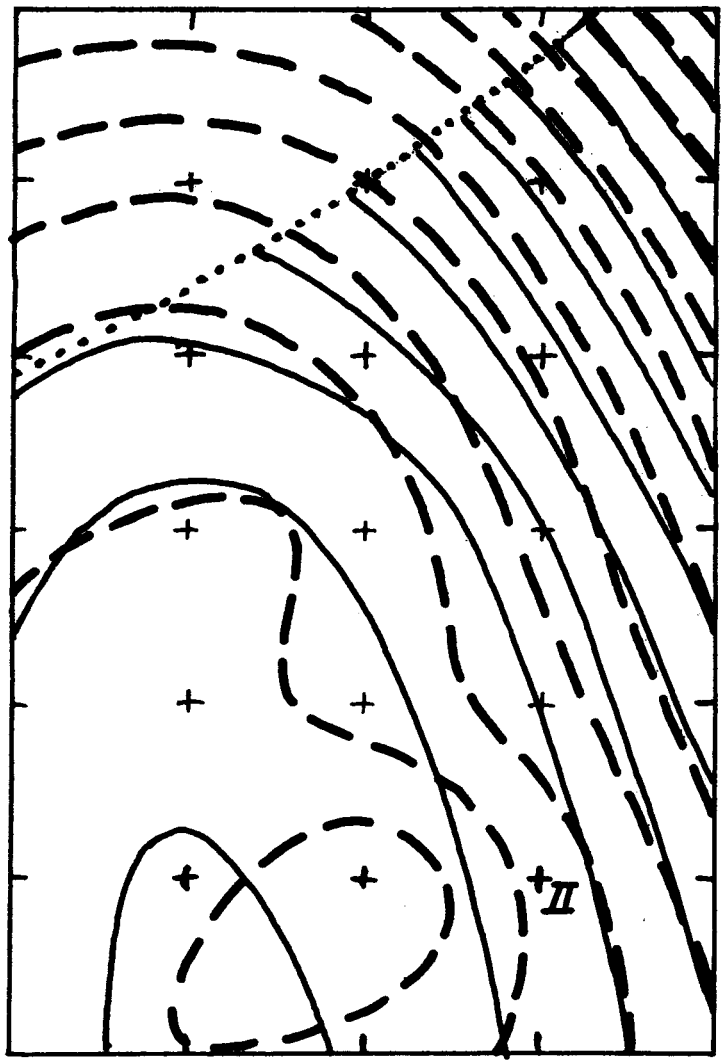

FIGURE 6.—Detailed structure of one of the two temporary irregularities which appeared on the Mercator grid. The isolines of z (for $t=36$ hours) are drawn on a Mercator projection, the small crosses being the points of Mercator grid A. The top of the figure is at $q=Q+1$. The heavy dashed isolines represent the Mercator analysis and the thin continuous lines an independent analysis of the corresponding stereographic grid. Both sets of isolines are drawn at intervals of 100 meters, the minimum value isolines in the upper right portion of the area being in both cases that for 8300 m. The grid point marked II is the point corresponding to curve II in figure 7.

and the vorticity of $\mathbf{v}_2$ is given by an equation similar to the balance equation (39), but with the non-linear terms in ψ evaluated geostrophically. Evidently Charney [3] and Hinkelmann [9] have each tested separately the value of adding to the geostrophic wind a correction either for the vorticity or for the divergence. The elimination of noise in both of their results is due to the special choice of initial

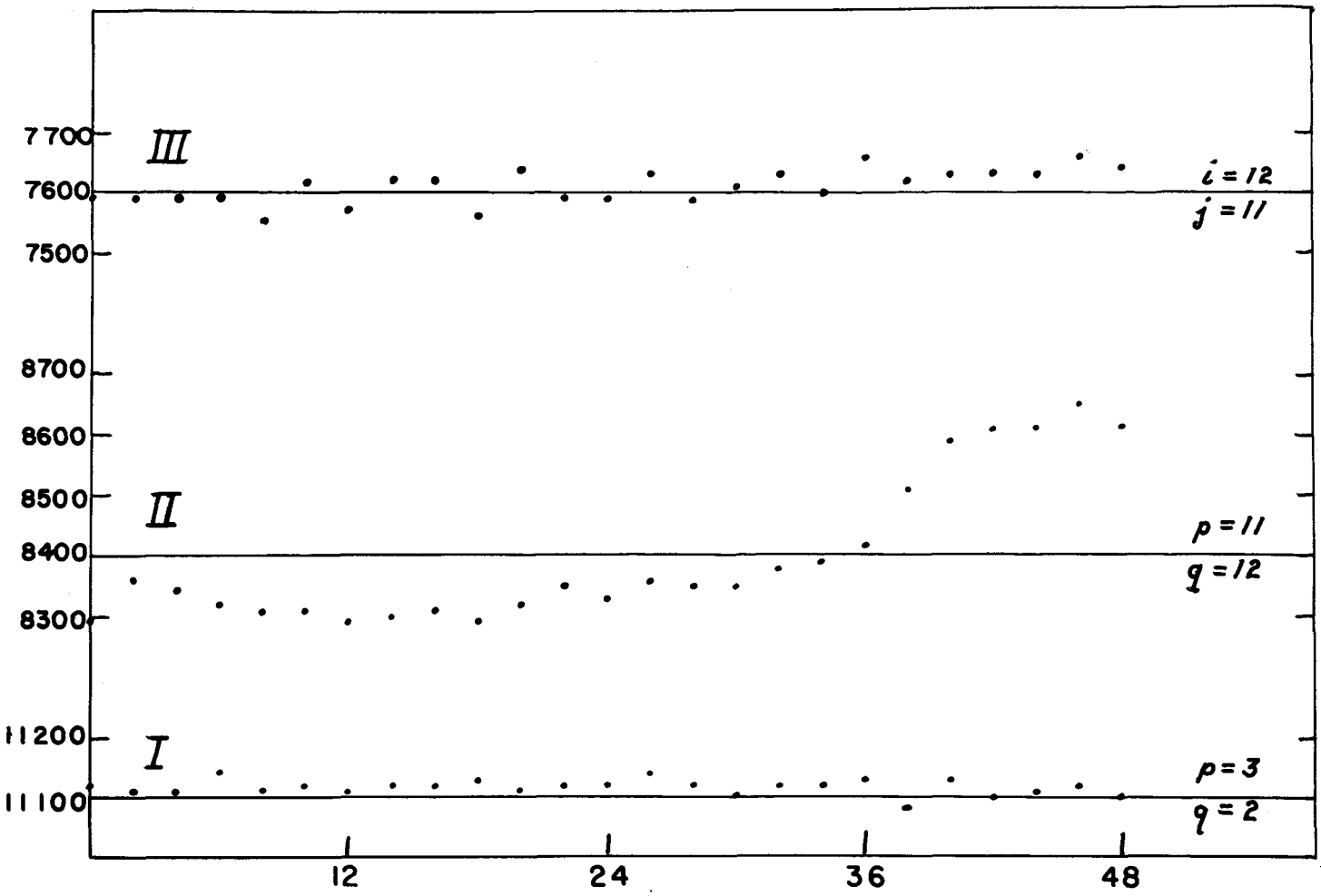

FIGURE 7.—Variation of the height of the free surface at three selected grid points, shown at 2-hour intervals. Units are meters.

data used by each of them; in Charney's special test case the correction for divergence was unnecessary, as mentioned above, because the wave was stationary, while in Hinkelmann's special case the linear terms in (39) were not only much larger than the neglected non-linear terms, but the correction for divergence was quite important because of the very strong baroclinicity in the zonal flow.

ACKNOWLEDGMENTS

The research described in this paper was sponsored by the Office of Naval Research and the Geophysical Research Directorate under contract Nonr 1841 (18). The computations were performed at the Computation Center of the Massachusetts Institute of Technology. Miss K. Kavanagh and Mr. A. Katz assisted in the programming of the computations.

REFERENCES

1. A. P. Burger, "Scale Considerations of Planetary Motions of the Atmosphere," *Tellus*, vol. 10, No. 2, May 1958, pp. 195–205.
2. J. Charney, "On the Scale of Atmospheric Motions," *Geofysiske Publikasjoner*, vol. 17, No. 2, 1948, 17 pp.
3. J. Charney, "The Use of the Primitive Equations of Motion in Numerical Prediction," *Tellus*, vol. 7, No. 1, Feb. 1955, pp. 22–26.
4. J. Charney, R. Fjørtoft, and J. von Neumann, "Numerical Integration of the Barotropic Vorticity Equation," *Tellus*, vol. 2, No. 4, Nov. 1950, pp. 237–254.
5. A. Eliassen, "The Quasi-Static Equations of Motion with Pressure as Independent Variable," *Geofysiske Publikasjoner*, vol. 17, No. 3, 1949, 44 pp.
6. A. Eliassen, *A Procedure for Numerical Integration of the Primitive Equations of the Two-Parameter Model of the Atmosphere*, Scientific Report No. 4, on Contract AF 19(604)–1286, Dept. of Meteorology, Univ. of California at Los Angeles, 1956, 53 pp.

7. B. Haurwitz, "The Motion of Atmospheric Disturbances on the Spherical Earth," *Journal of Marine Research*, vol. 3, 1940, pp. 254–267.
8. K. Hinkelmann, "Der Mechanismus des meteorologischen Lärmes," *Tellus*, vol. 3, No. 4, Nov. 1951, pp. 285–296.
9. K. Hinkelmann, "Ein Numerisches Experiment mit der primitiven Gleichungen," *C.-G. Rossby Memorial Volume*, Esselte A.B., Stockholm, 1959.
10. G. Hollman, "Über prinzipielle Mängel der geostrophischen Approximation und die Einführung ageostrophischen Windkomponenten," *Meteorologische Rundschau*, vol. 9, Nos. 5/6, May/June 1956, pp. 73–78.
11. E. N. Lorenz, "Static Stability and Atmospheric Energy," *Scientific Report*, No. 9, on Contract AF 19(604)–1000, (General Circulation Project), Dept. of Meteorology, Massachusetts Institute of Technology, 1957, 41 pp.
12. A. S. Monin, "Izmeneniîa Davleniîa v Baroklinnoi Atmosfere," [Pressure Changes in a Baroclinic Atmosphere] *Izvestiîa Akademiîa Nauk SSSR, Ser. Geofiz.*, No. 4, Apr. 1958, pp. 497–514.
13. N. A. Phillips, "A Map Projection System Suitable for Large-Scale Numerical Weather Prediction," *Journal of the Meteorological Society of Japan*, 75th Anniversary Volume, 1957, pp. 262–267.
14. G. Platzman, "The Computational Stability of Boundary Conditions in Numerical Integration of the Vorticity Equation," *Archiv für Meteorologie, Geophysik, und Bioklimatologie*, Ser. A, vol. 7, 1954, pp. 29–40.
15. G. Platzman, "The Lattice Structure of the Finite-Difference Primitive and Vorticity Equations," *Monthly Weather Review*, vol. 86, No. 8, Aug. 1958, pp. 285–292.
16. C.-G. Rossby and collaborators, "Relation Between Variations in the Intensity of the Zonal Circulation of the Atmosphere and the Displacements of the Semi-Permanent Centers of Action," *Journal of Marine Research*, vol. 2, 1939, pp. 38–55.
17. J. Smagorinsky, "On the Numerical Integration of the Primitive Equations of Motion for Baroclinic Flow in a Closed Region," *Monthly Weather Review*, vol. 86, No. 12, Dec. 1958, pp. 457–466.